

Influence of process-related heat accumulation of laser beam welded 1.7035 round bars on weld pool shape and weld defects

Cite as: J. Laser Appl. **33**, 042007 (2021); <https://doi.org/10.2351/7.0000478>

Submitted: 01 July 2021 . Accepted: 30 August 2021 . Published Online: 17 September 2021

 J. Grajczak,  C. Nowroth,  T. Coors, J. Twiefel,  J. Wallaschek, F. Saure, F. Pape, G. Poll,  S. Nothdurft, J. Hermsdorf,  V. Wesling, S. Kaierle, et al.

COLLECTIONS

Paper published as part of the special topic on [Proceedings of the International Congress of Applications of Lasers & Electro-Optics \(ICALEO® 2021\)](#)



View Online



Export Citation



CrossMark

ARTICLES YOU MAY BE INTERESTED IN

[Eddy current detection of laser-dispersed markers as a new approach to determining the position of load supporting means](#)

Journal of Laser Applications **33**, 042004 (2021); <https://doi.org/10.2351/7.0000486>

[Influence of plume attenuation under high power laser welding of copper using visible wavelengths](#)

Journal of Laser Applications **33**, 042006 (2021); <https://doi.org/10.2351/7.0000505>

[Shale gas permeability upscaling from the pore-scale](#)

Physics of Fluids **32**, 102012 (2020); <https://doi.org/10.1063/5.0020082>





LIA
THE LASER INSTITUTE

The professional society for
lasers, laser applications,
and laser safety worldwide.

Become part of the LIA experience -
cultivating innovation, ingenuity, and
inspiration within the laser community.



MEMBER

www.lia.org/membership
membership@lia.org

[Find Out More](#)

Influence of process-related heat accumulation of laser beam welded 1.7035 round bars on weld pool shape and weld defects

Cite as: J. Laser Appl. 33, 042007 (2021); doi: 10.2351/7.0000478

Submitted: 1 July 2021 · Accepted: 30 August 2021 ·

Published Online: 17 September 2021



J. Grajczak,¹ C. Nowroth,² T. Coors,³ J. Twiefel,² J. Wallaschek,² F. Saure,³ F. Pape,³ C. Poll,³ S. Nothdurft,¹ J. Hermsdorf,¹ V. Wesling,⁴ and S. Kaierle¹

AFFILIATIONS

¹Laser Zentrum Hannover e.V., Hollerithallee 8, 30419 Hannover, Germany

²Institute of Dynamics and Vibration Research, Leibniz University Hannover, An der Universität 1, 30823 Garbsen, Germany

³Institute of Machine Design and Tribology, Leibniz University Hannover, An der Universität 1, 30823 Garbsen, Germany

⁴Institute of Welding and Machining, Clausthal University of Technology, Adolph-Roemer-Straße 2a, 38678 Clausthal-Zellerfeld, Germany

Note: Paper published as part of the special topic on Proceedings of the International Congress of Applications of Lasers & Electro-Optics 2021.

ABSTRACT

The risk of weld defects increases when laser beam welding of round bars is performed in a rotational process. The reason is heat accumulation, which changes process conditions. The analysis of weld pool shape and weld defects in the course of a weld seam is essential for being able to evaluate the overall weld quality and to set up control measures. This study focuses on laser beam welding of round bars with partial welds and various welding speeds. The experiments are carried out with 1.7035 round bars of 30 mm diameter. For partial welds, a laser beam power of 6 kW and welding speed of 1 m/min are used for welding paths of 1/4, 1/2, and 3/4 of the circumference. Welding with various speeds is conducted with 0.5, 1.0, and 1.5 m/min and a constant energy per unit length of 240 kJ/m. The specimens are evaluated by metallographic micro-sections and scanning acoustic microscopy. The investigations reveal three major weld defects resulting from a gradient in linear welding speed between the specimen surface and the center and from heat accumulation due to specimen geometry. Porosity and hot cracks form under the surface and the weld root bulges, which also result in hot cracks. The weld depth increases to its final weld depth after approximately 1/8 of the circumference.

Key words: laser beam welding, steel alloy 1.7035, round bars, melt pool dynamics, hot cracking, bulging

Published under an exclusive license by Laser Institute of America. <https://doi.org/10.2351/7.0000478>

I. INTRODUCTION

The technology of welding round bars by laser is promising for the use of welding shafts. It differs strongly from other welding tasks like fillet welds, butt joints of sheets, and lap joints because round bars have to be welded around the circumference. Traditionally, rotary friction welding is used for welding round bars.¹ But it is disadvantageous that the workpiece length decreases during rotary friction welding and a flash forms around the weld. This can be avoided by using laser beam welding. Furthermore, laser beam welding processes are highly flexible and additional welding tasks could be carried out with the laser used and without the need of reclamping

the workpiece. But laser beam welding would need to be adapted to be used for round bars because the weld start and end points are the same, the bar center stays molten over the welding time, and the bar temperature increases continuously. As a result, the boundary conditions for welding and solidification are changing continuously, which complicates defect-free welding. Round bars welded by the laser are prone to hot cracking and gas porosity resulting from geometry and heat accumulation. Such defects significantly reduce the service life of components.

Hot cracks result from lately solidifying phases, which are given more time to form and segregate the higher the temperature

is. In a solidifying specimen, the solidification rate at its surface is higher than at its center, which results in internal stress during and after solidification. The weak and partially molten segregation areas can be pulled apart by this internal stress and hot cracks can form. The edges of hot cracks are coated by a segregated material.^{2,3} In areas of low internal stress and equiaxial solidification morphology, the risk of hot cracking is lower. Therefore, the segregated melt is spread over a larger area of grain borders than in directional solidification. In laser beam deep welding, three different solidification morphologies can be adjusted to influence hot cracking. At low solidification rates, the directionally solidified dendrites are pointing toward the weld surface, and the segregations are pushed ahead of the solidification front toward the specimen surface, preventing hot cracks. At medium solidification rates, the dendrites are parallel to the weld surface, and the segregations concentrate rectangularly to the surface and create hot cracks. At high solidification rates, the weld center solidifies equiaxially, and segregation from the outer directionally solidified dendrites can be distributed over a large area of grain boundaries, preventing hot cracks.⁴ In high-energy deep penetration welding, the melt pool can bulge. In this lately solidifying bulge, hot cracks can be caused due to solidification shrinkage.⁵

Gas porosity can result from an unstable and fluctuating keyhole.⁶ Keyholes can fluctuate due to unsteady melt flow, spatters, which absorb laser beam energy, and various other impacts. Hence, the keyhole bottom can be dissociated and gas from the keyhole can remain in the solidifying melt, creating gas porosity. With a bulging weld pool, gas porosity is more likely due to the geometrical obstruction of gas escape if gas is located in the bulge. Degassing is possible by gas ascension as long as the weld is liquid.^{7,8} In laser beam welding of round bars, this is supported by constantly increasing temperatures. But it is obstructed by its rotation. Therefore, gas porosity formation has to be prevented. In general, big keyholes are favorable due to better degassing properties, and slow melt pool convection is favorable due to less keyhole destabilization.^{9,10} By choosing adequate welding power and speed, fluctuations of the keyhole can be reduced. With the same energy per unit length, it is favorable to use higher welding power and speed for less weld porosity and, additionally, higher penetration depth.¹¹

The observation of keyhole and weld pool shapes in laser beam welding is possible by using x-ray imaging,¹² welding metals to transparent materials like quartz glass,^{13,14} or by interrupting the welding process.¹⁵ X-ray imaging and welding metals to transparent materials allow real-time observation of a keyhole, whereas stopping the welding process only allows preserving the keyhole shape. Dell Bello *et al.*¹⁵ successfully preserved the keyhole shape in welding austenitic stainless steel with a laser beam power of 10 kW and welding speed between 1.3 and 8 m/min. By analyzing metallographic longitudinal sections, they proved the possibility of keyhole shape preservation by interrupting the welding process using a mechanical switch. Artinov *et al.*¹⁶ investigated the differences between the weld end crater and the steady-state weld pool. After switching off the laser beam, the base material in front of the weld pool can continue melting, while the weld material at the back of the weld pool solidifies. As a result, the shape of the end crater can differ from the shape of the steady-state weld pool.

TABLE I. Chemical composition of 1.7035 steel alloy in wt. % (Ref. 19).

C	Si	Mn	Cr	S
0.420	0.250	0.700	1.050	<0.035

From previous experiments,^{17,18} it is known that a large melt pool can form in the center of a round bar, containing porosity and cracks. But it is not known how the laser beam welding behavior changes with increasing weld length and heat accumulation. Hence, two kinds of tests are conducted. First, round bars are welded partially to freeze the respective weld status and identify the current and developing weld seam shape and weld defects. These specimens are evaluated by metallographic longitudinal sections. Second, round bars are welded with different welding speeds and laser beam powers at a constant energy per unit length to identify the influence on melt pool dynamics and weld pool behavior. These specimens are evaluated by scanning acoustic microscopy regarding weld depth and weld defects. To trigger weld defects, 41Cr4 (1.7035) is used as the material for the specimens. It is prone to cracking because of its high hardenability due to high carbon and chromium content, see Table I.

II. EXPERIMENTAL SETUP

The laser beam welding tests were conducted with a diode-pumped solid state disk laser system (TruDisk 16002, TRUMPF GmbH + Co. KG) and specifications according to Table II.

The laser processing head is held in a static fixed position by a robot system (KR 60 HA, Kuka AG), while the welding speed is provided by rotating the specimen, see Fig. 1. The detailed setup description is available in Ref. 20.

III. EXPERIMENTAL PROCEDURE

Round bars with a diameter of 30 mm made of steel alloy 1.7035 are used as specimens for all bead on plate welds. To impede the formation of melt drops, the processing head is tilted by 20°, and the laser focus point is positioned 6 mm backward from the angular point over the specimen's surface. It is adjusted to be 4 mm below the specimen surface. Argon shielding and process gas is provided by two flat nozzles with a pressure of 6 bar and a flow rate of 60 l/min at an angle of 45°. They are positioned with 50 mm distance to each other and to the specimen and directed at the specimen bottom and above it. The general process parameters

TABLE II. Specifications for the laser beam welding setup.

Laser beam source	TruDisk 16002
Wavelength (nm)	1030
Optical fiber diameter (μm)	200
Collimation length (mm)	150
Focal length (mm)	300
Focal spot diameter (μm)	400

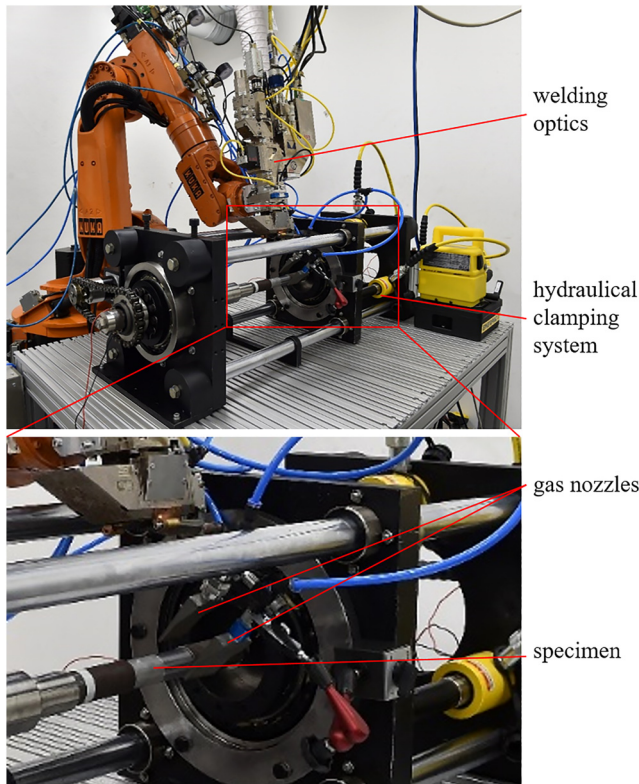


FIG. 1. Experimental setup for laser beam welding.

are determined by previous experiments.^{18,21,22} Two kinds of tests are conducted, partial welding and welding with different speed.

For partial welding, a laser beam power of 6 kW and a welding speed of 1 m/min are used. According to the test plan in Table III, the specimens are welded with different distances along the round bar circumference to save the respective weld status at the weld start, middle, and near its end. The laser irradiation stops at the respective circumference ratio, but the specimen rotates for the whole circumference.

For full circumference welds with different speed at a constant energy per unit length, parameters according to Table IV are used. For calculation of the cooling rate, the temperature is recorded by a thermographic camera (VarioCAM head HiRes 640, Jenoptik AG) at a laser beam power of 6 kW and a welding speed of 1.5 m/min. The camera is positioned horizontally behind the weld start point to avoid disturbances and damage by spatters, and the measurement point is placed 25 mm after the weld start point.

Metallographic longitudinal sections of the partial welding specimens are prepared. The etching is conducted with 3% Nital

TABLE III. Test plan for partial laser beam welding of round bars.

Weld length as circumference ratio	1/4	1/2	3/4
Number of specimens	3	3	3

TABLE IV. Test plan for round bar welding with different speed.

Welding speed (m/min)	0.5	1.0	1.5
Laser beam power in kW	2	4	6
Number of specimens	3	3	3

etchant, consisting of 97 ml H₂O and 3 ml HNO₃, for 10 s. The specimens welded with varying welding speed are cut longitudinally close to the weld seam, polished, and investigated by scanning acoustic microscopy, as described in Ref. 23. The basic principle is that a scanner-mounted transducer emits sound waves in the ultrasonic range ($f > 20$ kHz), which are transmitted into a specimen and reflected on interfaces or a medium of different densities and acoustic impedances (i.e., pores, cracks, or inhomogeneities) there. Distilled water is used as the coupling medium between the specimen and the transducer. The reflected signals are received by the

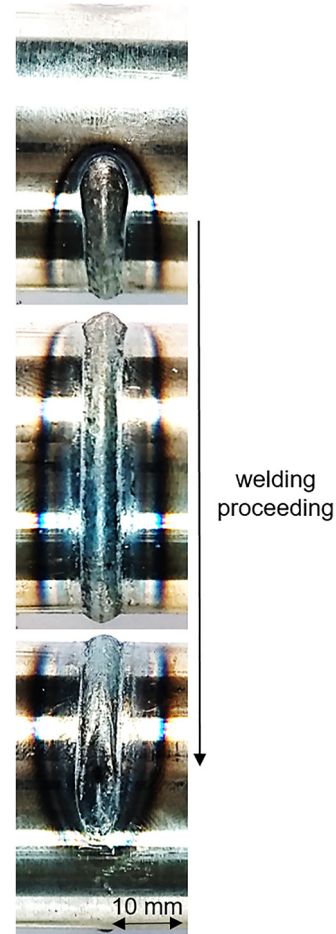


FIG. 2. Exemplary weld seam inspection, weld along 3/4 circumference.

transducer, and the information obtained from them is used to generate an image of the specimen's subsurface structure (C-scan through the impulse echo method). Transducers with frequencies of 30 and 75 MHz with focus lengths of 12.7 and 20 mm, respectively, are selected. Multiple gates in the z direction with a length of 25 ns each, which corresponds to a resolution of 75 μm in the depth direction, are chosen.

IV. EXPERIMENTAL RESULTS

A. Partial welding

For comparing the longitudinal metallographic sections, the outer weld seam appearance is displayed exemplarily in Fig. 2.

From the weld start, weld reinforcement is visible, and a crater forms at the weld end. The weld seam is broadly surrounded by annealing colors. At the weld start and the end, the width of annealing colors is smaller.

By analyzing the micrographs, see Fig. 3, a big variety of effects at different welding stages is shown.

From the weld start until approximately 1/8 of the circumference, the weld depth increases to its final weld depth.

While the laser focus diameter is 400 μm, the weld pool diameter at its narrowest position is about 500 μm. In one micrograph, a

cavity is visible, but in the other micrographs a metal area, which contains a lot of cracks and has a similar shape to the cavity is visible. The end crater is an area with high susceptibility for cracking.¹⁶

For a detailed inspection of weld pool evolution, the weld pool shapes are compared in Fig. 4.

With increasing weld length, weld depth and bulging area increase. From 1/4 circumference to 1/2, the difference is high, but from 1/2 to 3/4, the weld pool shape changes marginally. Hence, between weld lengths of 1/4 and 1/2, enough heat accumulates to influence the weld pool shape and enhance weld pool bulging.

Specific phenomena regarding solidification as well as porosity and crack formation will be discussed in detail in the following paragraphs. Solidification lines are visible in the longitudinal sections, see Fig. 5.

Hot cracks are located at the weld top and the bottom area along the solidification lines. In between them, small cracks and pores can be found. The bottom cracks result from weld pool bulging, which results in a lately solidifying area with an increased risk of solidification cracking. The top cracks in the longitudinal sections of the steel alloy are located in the broad weld top, which is shown in the exemplary metallographic cross section in Fig. 6.

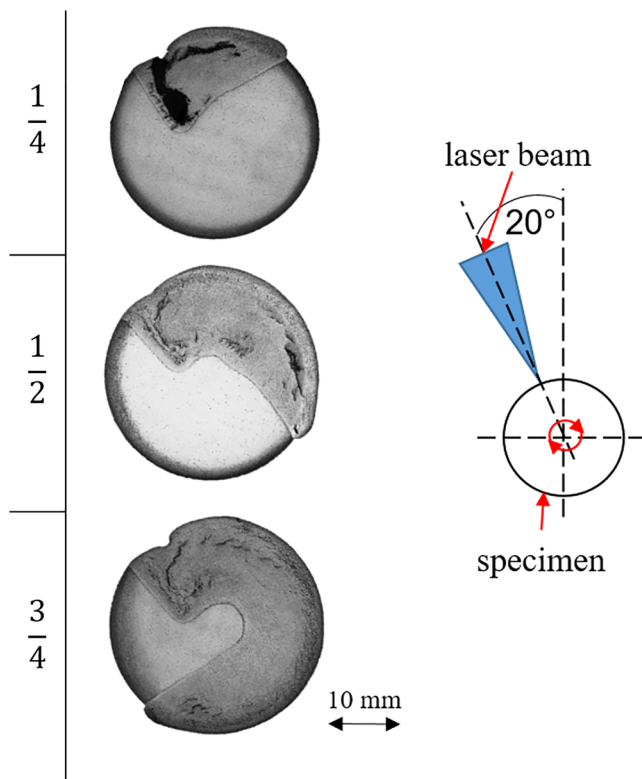


FIG. 3. Exemplary micrographs of metallographic longitudinal sections of 1.7035 weld seams at different circumference welding ratios, with welding scheme.

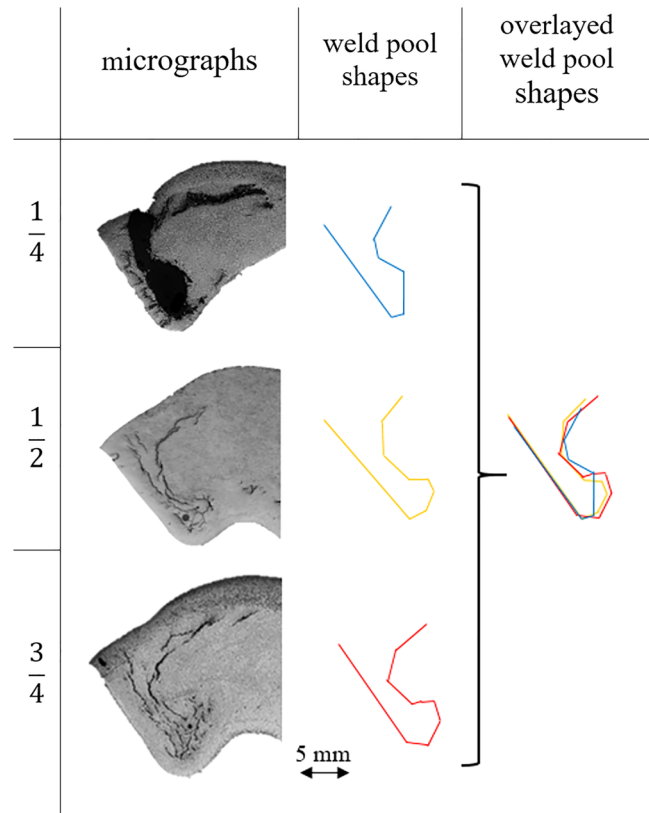


FIG. 4. Abstraction and comparison of weld pool shapes from longitudinal cross sections at different circumference weld ratios.

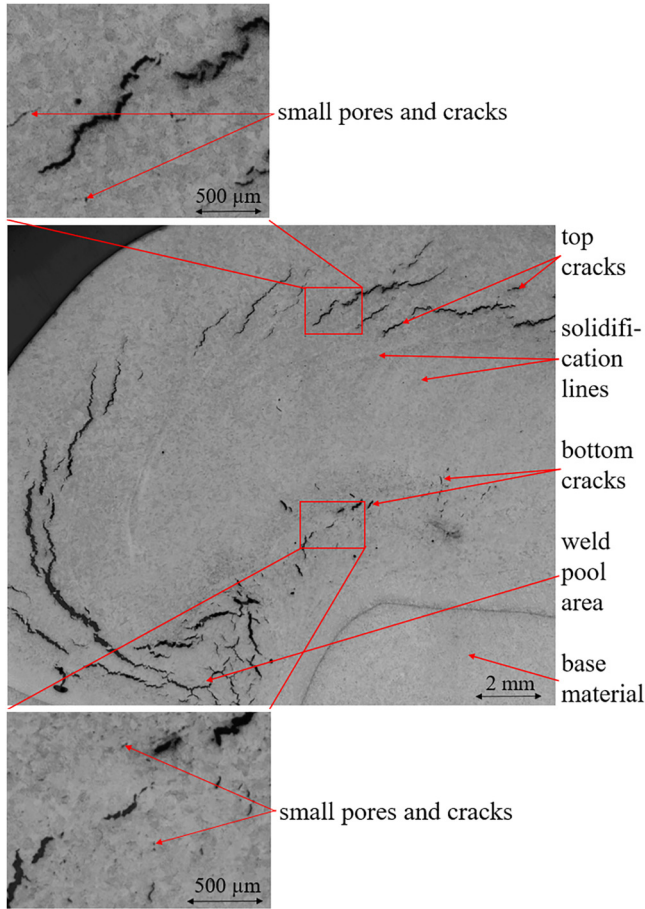


FIG. 5. Detailed view of a longitudinal section, 1/2 circumference weld.

The cracks form due to gradients of solidification speed and resulting stress.

Additionally, the geometrical influence on stress in the welding of round bars has to be considered because the given

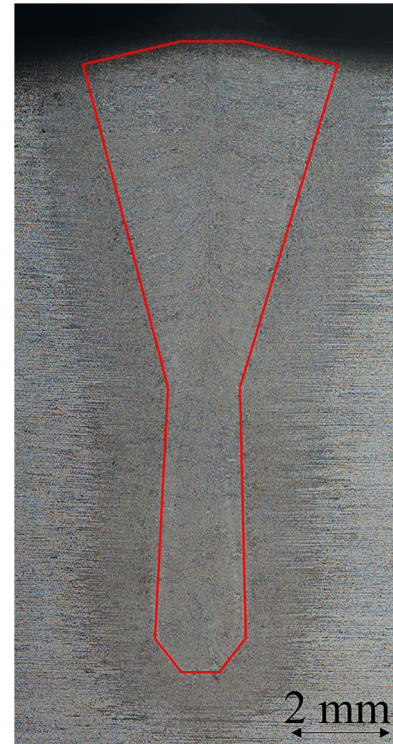


FIG. 6. Exemplary cross section of a laser beam-welded round bar.

welding speed equals the angular speed and not the linear speed. From the specimen surface to its center and increasing weld depth, the linear speed decreases. If the round bar is welded through, its center stays molten over the whole welding time and heat accumulates. This heat accumulation in the weld center in addition to heat accumulation over welding time supports bulging, solidification cracking, and pore formation in the root area. Furthermore, the solidification stress does not result in cold cracks. It is consumed during solidification by hot crack formation.

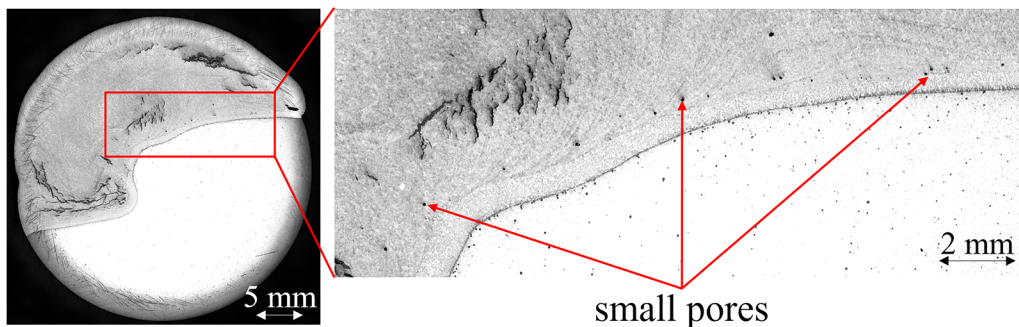


FIG. 7. Detailed view of a longitudinal section regarding root porosity.

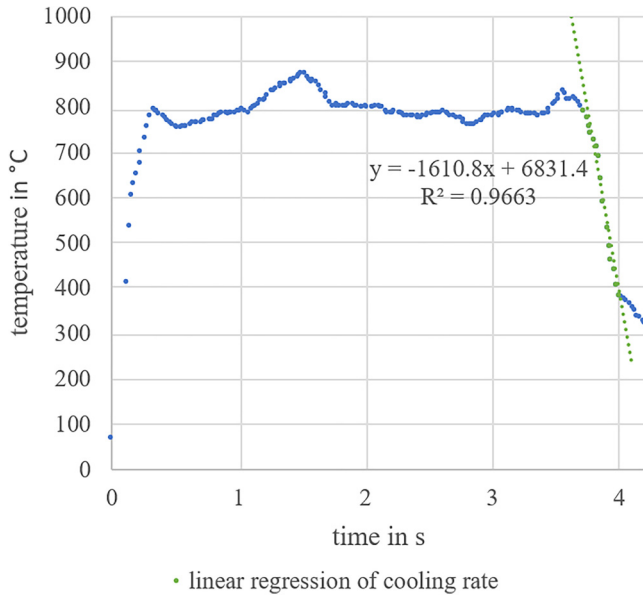


FIG. 8. Temperature curve and determination of the cooling rate, measurement point placed 25 mm after the weld start point, laser beam power of 6 kW, and welding speed of 1.5 m/min.

Small pores are located at the weld root due to keyhole instabilities, see Fig. 7.

The keyhole stability is influenced by various welding speed over the weld depth. The high welding speed at the surface results in a fast melt flow, which could destabilize the keyhole. But the present micrographs reveal only small top porosity. The low welding speed at the round bar center results in a slow melt flow, which effects less keyhole destabilization on the one hand, but on the other hand, less heat is carried to the weld top and bulging is increased.

A cooling rate of 1611 K/s is found by thermographic measurements, see Fig. 8. 25 mm behind the weld start point, the weld temperature fluctuates between 780 and 880 °C.

B. Welding with varying speed

Different weld behaviors for various welding speeds can be seen in the scanning acoustic micrographs, see Fig. 9.

The weld edge is shown at a lower scanning depth of the ultrasonic microscope, and the weld center is shown at a higher scanning depth. In spite of constant linear energy, the weld depth increases with increasing laser beam power.

For 0.5 m/min and 2 kW, a low amount of cracks and much small gas porosity is located at the weld root and the center. The keyhole can be assumed to be unstable and to fluctuate. For 1.0 m/min and 4 kW, many little defects are located at the weld top and a high amount of cracks is located in the whole weld seam. The indications of small porosity can be a mixture of small cracks and porosity like in Fig. 5. The weld pool is larger and, again, the top porosity can result from destabilization by a fast melt flow at

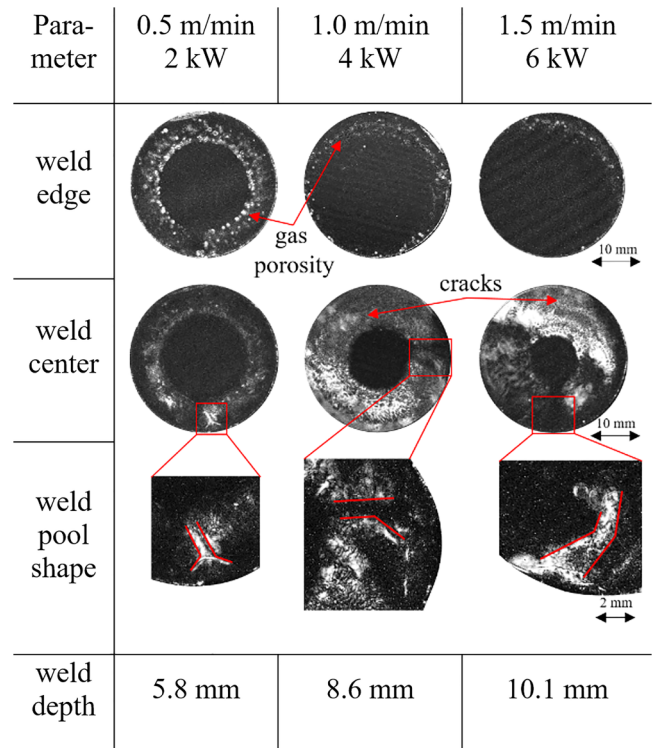


FIG. 9. Exemplary scanning acoustic micrographs of 1.7035 weld seams welded with varying speed and exemplary emphasized weld pool shapes.

its top due to differing angular speed. In addition, cracks are caused by a high solidification stress due to a high amount of melt. For 1.5 m/min and 6 kW, again some little gas porosity and many cracks are located at the weld edge. In the weld center, cracks are located mainly at the top and bottom, see Fig. 10. The weld pool is large with keyhole destabilization at the top and a large bulging

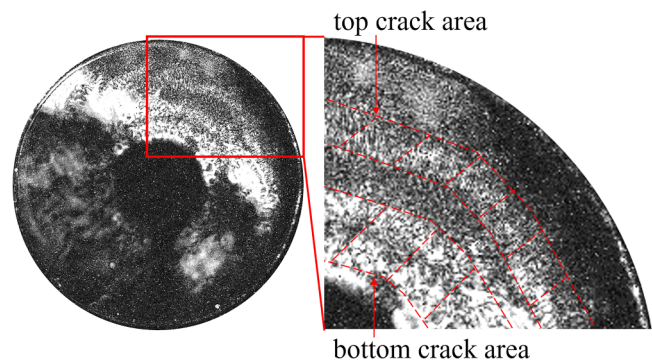


FIG. 10. Exemplary scanning acoustic micrograph of 1.7035 weld seam, welding speed of 1.5 m/min and welding power of 6 kW.

TABLE V. Weld defects and causes in laser beam welding of round bars with partial penetration.

Weld defect	Cause
Top cracks	Gradient of solidification speed from the surface to the center (cf. Figs. 5 and 10)
Top porosity	Gradient of welding speed from the surface to the center and keyhole destabilization (cf. Fig. 9)
Bottom cracks and porosity	Weld pool bulging due to heat accumulation (cf. Figs. 4, 5, and 10)

area resulting in a separate bottom crack area. In addition to the previous longitudinal sections, the presence of porosity at the weld top is revealed by the scanning acoustic microscopy images.

V. CONCLUSIONS

The weld depth increases to its final weld depth from weld start until approximately 1/8 of the circumference, but no unwelded area remains due to the overlapping of weld start and end. After 1/4 of the circumference, enough heat is accumulated in the specimen and weld pool bulging begins.

Several typical weld defects in laser beam welding of round bars were identified, see Table V.

In laser beam welding of round bars, the linear speed at the specimen surface is higher than at its center. As a result, the speed of the melt flow near the surface is higher, and it is more likely that gas from the keyhole is retained in the weld. In the specimen center, the low linear speed results in heat accumulation, bulging, cracks, and porosity.

Scanning acoustic microscopy is an appropriate instrument for detailed inspections of round bar welds and for the identification of weld pool shapes. The weld pool size and keyhole stability increase with increasing welding speed and weld depth at a constant linear energy.

VI. OUTLOOK

The identified weld defects match the defects of full penetration welding, cf. Refs. 17 and 18. Therefore, the bulging area is located in the bar center and results in central cracks and porosity. Therefore, the central defect could be removed by generating a bulge-free weld pool and by minimizing the weld depth for full penetration.

The top porosity should be similar for full penetration welding. It could be removed by improving degassing or stabilizing the keyhole top. The top cracks could be removed by reducing the solidification stress gradient.

In future investigations, ultrasonic excitation and laser beam power modulation will be applied. By ultrasonic excitation, the keyhole top can be stabilized^{20,21} and cracks can be removed due to enhanced mixing.^{17,18,22} By laser beam power modulation with a high frequency, the weld pool bulging as well as porosity and cracks can be reduced.^{11,12} By using a low frequency, it could be possible to switch the weld depth periodically between full and

partial penetration but overlap the full penetration sections to achieve an overall full penetration. Removing the top cracks by a second melting with low weld depth and speed would not be trivial due to the risk of porosity, see Fig. 9.

To identify the influence of various welding speeds on the weld quality, further tests with a constant weld depth are necessary. To remove the remaining end craters, laser beam power has to be ramped down.

ACKNOWLEDGMENTS

The authors would like to acknowledge the German Research Foundation (DFG) for the financial and organizational support of this project. Funded by the Deutsche Forschungsgemeinschaft (DFG, German Research Foundation)—CRC 1153, subproject A3-252662854.

REFERENCES

- H. S. Kim, D. P. Hong, S. M. Yang, and H. Y. Kang, "Tensile strength characteristic of Al6061-T6 and Al7003-T6 aluminum by the change in the friction welding process variable," *Appl. Mech. Mater.* **532**, 534–539 (2014).
- H. Krafka, Risse in Schweißverbindungen: Heißrisarten, Heißrisentstehung und Heißrisprüfung, in 32. Tagung des DVM-Arbeitskreises Bruchvorgänge, 22. und 23. Februar 2000 in Berlin, Berlin, 161–172 (2000) (in German).
- J. C. Wendt, Merkblatt DVS 1004-1: Heißrisprüfverfahren Grundlagen, DVS Media GmbH (1996) (in German).
- J. Schuster, "Heißrisse in schweißverbindungen: Entstehung, nachweis und vermeidung, theoretische beschreibung der heißrisanfälligkeit metallischer werkstoffe unter besonderer berücksichtigung hochlegierter stähle und nickellegierungen, DVS-berichte," Ph.D. thesis, Verl. für Schweißen und Verwandte Verfahren, DVS-Verl., 2004 (in German).
- A. Artinov, M. Bachmann, X. Meng, V. Karkhin, and M. Rethmeier, "On the relationship between the bulge effect and the hot cracking formation during deep penetration laser beam welding," *Procedia CIRP* **94**, 5–10 (2020).
- A. Matsunawa, "Problems and solutions in deep penetration laser welding," *Sci. Technol. Weld. Joining* **6**, 351–354 (2001).
- S. Katayama, N. Seto, J. D. Kim, and A. Matsunawa, "Formation mechanism and suppression procedure of porosity in high power laser welding of aluminum alloys, in Laser Institute of America-Proceedings-LIA," *Laser Mater. Process. Conf.* **85**, C-24–C-33 (1998).
- J. Volpp, "Keyhole stability during laser welding—Part II: Process pores and spatters," *Prod. Eng.* **11**, 9–18 (2016).
- M. Beck, *Modelling of Deep Penetration Laser Welding* (Teubner, Stuttgart, 1996).
- P. Stritt, "Prozessstrategien zur vermeidung von heißrisen beim remote-laserstrahlschweißen von AlMgSi 6016," Dissertation, Universität Stuttgart, 2016 (in German).
- A. Heider, *Erweitern der Prozessgrenzen beim Laserstrahlschweißen mit Einschweißstiefen zwischen 1 mm und 10 mm* (Herbert Utz Verlag GmbH, Munich, Stuttgart, 2018) (in German).
- M. Schaefer, S. Kessler, P. Scheible, N. Speker, and T. Harrer, "Hot cracking during laser welding of steel: Influence of the welding parameters and prevention of cracks," in *High-power Laser Materials Processing: Applications, Diagnostics, and Systems VI*, San Francisco, CA, 22 February 2017 (SPIE, San Francisco, CA, 2017), p. 100970E.
- W. M. Steen, J. Mazumder, and J. Mazumder, *Laser Material Processing 4* (Springer, London, 2010).
- J. L. Zou, S. K. Wu, W. X. Yang, Y. He, and R. S. Xiao, "A novel method for observing the micro-morphology of keyhole wall during high-power fiber laser welding," *Mater. Design* **89**, 785–790 (2016).

¹⁵U. del Bello, C. Rivela, M. Cantello, and M. Penasa, "Energy balance in high power CO2 laser welding," *Proc. SPIE* **1502**, 104–116 (1991).

¹⁶A. Artinov, V. Karkhin, M. Bachmann, and M. Rethmeier, "Mathematical modeling of the geometrical differences between the weld end crater and the steady-state weld pool," *J. Laser Appl.* **32**, 022024 (2020).

¹⁷B.-A. Behrens, A. Chugreev, T. Matthias, S. Nothdurft, J. Hermsdorf, S. Kaierle, H. Ohrdes, J. Twiefel, J. Wallaschek, M. Mildebrath, and T. Hassel, "Investigation of the composite strength of hybrid steel-steel semi-finished products manufactured by laser beam welding and friction welding," in *IOP Conference Series: Materials Science and Engineering*, 14 November 2018 (Pilsen, Czech Republic, Gottfried Wilhelm Leibniz Universität Hannover, Hannover, 2018).

¹⁸S. Nothdurft, H. Ohrdes, J. Twiefel, J. Wallaschek, J. Hermsdorf, L. Overmeyer, and S. Kaierle, "Investigations on the effect of different ultrasonic amplitudes and positions in the vibration distribution on the microstructure of laser beam welded stainless steel," in *High-Power Laser Materials Processing: Applications, Diagnostics, and Systems IX*, San Francisco, CA, 2 March 2020 (SPIE, San Francisco, CA, 2020), p. 112730J.

¹⁹VDM Metals, Datenblatt No. 4118: VDM Alloy 625, VDM Metals (2018).

²⁰H. Ohrdes, S. Nothdurft, C. Nowroth, J. Grajczak, J. Twiefel, J. Hermsdorf, S. Kaierle, and J. Wallaschek, "Influence of the ultrasonic vibration amplitude on the melt pool dynamics and the weld shape of laser beam welded EN AW-6082

utilizing a new excitation system for laser beam welding," *Prod. Eng.* **15**, 151–160 (2021).

²¹J. Grajczak, C. Nowroth, S. Nothdurft, J. Hermsdorf, J. Twiefel, J. Wallaschek, and S. Kaierle, "Influence of ultrasound on pore and crack formation in laser beam welding of nickel-base alloy round bars," *Metals* **10**, 1299 (2020).

²²S. Nothdurft, H. Ohrdes, J. Twiefel, J. Wallaschek, M. Mildebrath, H. J. Maier, T. Hassel, L. Overmeyer, and S. Kaierle, "Influence of ultrasonic amplitude and position in the vibration distribution on the microstructure of a laser beam welded aluminum alloy," *J. Laser Appl.* **31**, 022402 (2019).

²³F. Pape, T. Coors, T. Matthias, B.-A. Behrens, and G. Poll, "Ultrasonic evaluation of tailored forming components," *Bear. Steel Technol.* **12**, 300–312 (2020).

Meet the Author

Jan Grajczak studied material engineering at the Clausthal University of Technology. Since 2019, he has been at the Laser Zentrum Hannover e.V. as a research assistant in the group Joining and Cutting of Metals in the department Materials and Processes. His main research subject is ultrasonic assisted joining of round bars.